Hindawi

Research Article

The Interannual Relationship between the Diabatic Heating over the South Asia and the Snow Depth over the Southern Tibetan Plateau in Late Spring to Early Summer: Roles of the Air Temperature

Chengyang Zhang [ID]**,**[1] **Zhihai Zheng** [ID]**,**[2] **Yi Ou,**[1] **Tuantuan Zhang,**[3,4] **Zhixiang Xiao,**[1] **Sheng Lai,**[1] **Yuexing Cai,**[1] **Sirong Chen,**[1] **Weijian Qin,**[1] **and Hui He**[1]

[1]*Climate Center, Guangxi Meteorological Bureau, Nanning 530022, China*
[2]*Laboratory for Climate Studies, National Climate Center, China Meteorological Administration, Beijing 100081, China*
[3]*School of Atmospheric Sciences, Sun Yat-sen University, Southern Laboratory of Ocean Science and Engineering, Zhuhai 519082, China*
[4]*Guangdong Province Key Laboratory for Climate Change and Natural Disaster Studies, Sun Yat-sen University, Zhuhai 519082, China*

Correspondence should be addressed to Zhihai Zheng; zhengzh@cma.gov.cn

The southern Tibetan Plateau (TP) is snow covered during cold season but exhibits faster snow melting in early summer. Using in situ observations and improved satellite-derived data, the present study indicates that the snow depth (SD) over the southern TP exhibits distinction characteristics between late spring (i.e., P1: April 16th–May 15th) and early summer (i.e., P2: May 16th–June 14th). In terms of climate states, the snow melting rate over the southern TP in P2 is faster than that in P1. The acceleration of snow melting during P2 is mainly found over high elevation areas caused by the increase of local air temperature. Diagnoses of the thermodynamic equation further demonstrate that the warming over the southern TP during the two periods is mainly attributed to the meridional temperature advection and diabatic heating in situ. On the interannual time scale, the SD over the southern TP is closely related to diabatic heating over South Asia. During P1, the diabatic cooling from the southern Bay of Bengal eastward to the western South China Sea suppresses convection over the Bay of Bengal and southern TP and has resulted in an upper-level anomalous cyclone and cold temperature anomalies from the surface to 200 hPa over the southern TP, favoring the above-normal SD over the southern TP. On the other hand, SD over the southern TP in P2 is closely related to diabatic cooling over the northern Indochina Peninsula and diabatic heating over the southern China. But we could not prove that these diabatic heating anomalies can affect the SD over the southern TP by modulating local surface air temperature. This may be limited by the quality of the data and the simulation capability of the simple model.

1. Introduction

The Tibetan Plateau (TP) snowpack is considered to be an important factor modulating a regional hydrological cycle and exerts great impacts on agriculture and industry in populous Asia [1–7]. From the perspective of the annual cycle, the snow depth (SD) over the TP begins to increase in autumn and gradually melts during the following spring and summer [8, 9]. It is worth mentioning that some high elevation areas (e.g., the western TP) are covered with snow all year round [10]. The annual cycle of SD is closely related to local temperature. The out-of-phase variation of 2-m air temperature and SD over the TP was found in a station dataset [11]. The snow albedo effect is one of the dominant

causes of local temperature and SD variations [12]. The absorbed solar radiation over the snow-covered area led to the increase of underlying surface temperature and hence snow melting [13], and the snow albedo effect gradually decreases [14]. A recent study [15] confirmed that the deposition of absorbing aerosols from Taklimakan desert to populous Ganges plain induces decrease of the snow albedo effect by causing a positive radiative effect on snow, resulting in the reduced snow cover over the northern TP slopes during premonsoon season.

Surface temperature and snowfall are the important factors that directly affect the year-to-year variability of SD [16–20]. Wang et al. [21] showed that in autumn, the eastern North Pacific and western North Atlantic Sea surface temperature anomalies excited southeastward propagating wave train, which led to snow cover anomalies by causing anomalous snowfall. In winter, Indian Ocean Dipole (IOD) and El Niño-Southern Oscillation (ENSO) induced anomalous moisture transported to the TP through different mechanisms. The water vapor transport directly affected snowfall and then regulated SD over the TP [11]. However, in spring and summer, some studies [17, 18] proposed that snowfall contributed little to snow cover anomalies over the TP and the dominant factor is surface temperature. The surface temperature over the TP is closely related to the onset of Indian summer monsoon [22], which is mainly influenced by the strongest diabatic heating in May over the Bay of Bengal and Indochina Peninsula [23–25]. Senan et al. [22] suggested that negative (positive) SD anomalies over the TP is accompanied by the strongest (weak) diabatic heating around Indochina Peninsula which is closely related to the monsoon onset anomalies. The condensation heating over South Asia is usually accompanied by large-scale convective precipitation, resulting in variations of the local temperature gradient around the TP [26–28]. In addition, Jiang et al. [29] showed that the interannual variation of latent heat release of condensation over the TP is obviously affected by tropical convection near Indochina Peninsula during boreal summer.

The studies of temporal and spatial snow cover are constantly being refined [30–34]. For the eastern part of the Nyainqêntanglha Mountains, the annual cycle of snow cover is the most dominant component and explains at 76.6% of the total variability [35]. Although the southern TP (including the Nyainqêntanglha Mountains) occupies only small part of the plateau, it is a prominent area of TP heating in summer and has significant impacts on the surrounding weather and climate [36–39]. From the perspective of climate states from the station dataset, most snow-free stations are concentrated in the southern part of the TP in summer [18]. Compared with the central and eastern TP, this is a unique phenomenon in this region. Note that both thermal and mechanical forcing types over the southern TP play an important role in the formation and evolution of the South Asian summer monsoon [40–42]. However, the effect of diabatic heating over South Asia on SD over the southern TP is unclear during spring-summer transitional season. In order to further analyze the characteristics of regional SD, two scientific questions will be addressed. (1) The evolution

characteristics of SD and air temperature over the southern TP in late spring to early summer. (2) The interannual relationship between the diabatic heating over South Asia and SD over the southern TP during a different snow melting period: roles of the air temperature.

The present paper is organized as follows: Section 2 describes the data and model. According to the evolution characteristics of climatological SD, the features of temperature related to SD in different snow melting periods will be analyzed in Section 3.1. In Section 3.2, we investigate the influences of diabatic heating over South Asia on the year-to-year variability of SD over the southern TP. The underlying mechanisms are examined. The discussion and conclusions of the main findings are provided in Section 4 and Section 5, respectively.

2. Data and Methods

2.1. Observation. The station observation daily data of 2-m air temperature and SD for the period of 1979–2011 in China from the China Meteorological Administration (CMA) are used in this work. Due to the insufficient number of observation stations over the southern TP, extra daily SD data with a resolution of $0.25° × 0.25°$ during 1979–2004 from Dai and Che [43] are also applied, which are relatively more reliable than passive microwave sensors data in different satellite platforms [44]. Daily atmospheric reanalysis data (e.g., air temperature, geopotential height, winds, omega at multiple levels, and surface pressure) from National Centers for Environment Prediction/National Center for Atmospheric Research (NCEP/NCAR) during 1979–2004 are applied in this work. In order to analyze the characteristics of SD evolution in late spring to early summer, April-May-June (AMJ) is divided into 18 pentads, excluding June 30, for example, pentad-1 corresponding to April 1–5, pentad-2 corresponding to April 6–10, pentad-3 corresponding to April 11–15 - . . .. The southern TP SD index (SSDI) is defined as the SD anomalies averaged over the areas (28°–32°N, 88°–98°E) by using satellite-derived data [43, 44]. For further analyzing the contributions of physical processes to the local temperature variations, the thermodynamic equation [45] is applied as follows:

$$\frac{\partial T}{\partial t} = -V \bullet \nabla T - \left(\frac{P}{p_0}\right)^{R/C_P} \omega \frac{\partial \theta}{\partial p} + \frac{Q1}{C_P}. \qquad (1)$$

In equation (1), the four terms from left-hand to right-hand are local temperature variation, horizontal temperature advection, vertical temperature advection, and diabatic heating, respectively. T is the air temperature; V is the horizontal velocity; p and $p0$ are the pressure and surface pressure, respectively; ω is the vertical pressure velocity; R is the gas constant; C_p is the specific heat of dry air at constant pressure. θ and Q1 are the potential temperature and the apparent heat source, respectively.

2.2. Model. A nonlinear baroclinic model is applied in this study to confirm the potential role of atmospheric temperature in relationship between the diabatic heating

anomalies over South Asia and SD over the southern TP. The model is designed as 24 sigma levels in the vertical and spectral R30 horizontal resolution. For more details about the nonlinear baroclinic model, one may refer to Ting and Yu [46]. The solution of the model is stable after about 15 days. Therefore, the model is integrated for 60 days, and only the average of the last 20 days is analyzed in this study. The specific experimental design for this study will be detailed in Section 3.2.

The nonlinear baroclinic model is widely used in the research community of atmospheric science [11, 46]. The simplified dynamical framework facilitates interpreting the responses of perturbations in the large-scale atmospheric dynamics, compared to the complicated atmospheric general circulation models. Additionally, the model is ideal for studying the fundamental mechanisms underlying atmospheric dynamics, such as Rossby waves, atmospheric teleconnection patterns, and baroclinic instability. However, the moist processes, e.g., large-scale condensation and convection, are not included in the model, which is not sufficient to discuss interactions between dynamics and convection. The nonlinear baroclinic model employed in this study is a time-dependent, dry, and primitive equation anomaly model.

3. Results

3.1. The Characteristics of SD and Air Temperature Evolution over the Southern TP from Late Spring to Early Summer. The stations above 2500 m are mainly concentrated in the eastern TP (25.5°–40°N, 85°–105°E). According to Xu et al. [18], the southern TP is outlined by the red box (28°–32°N, 88°–98°E) in Figure 1, which contains 28 in situ stations. The quality control (the missing value should be fewer than 7 days) is carried out for station data over the southern TP. Only 14 stations are finally picked out in this study during 1979–2004. The station locations are marked by a blue cross in Figure 1. Table 1 shows the specific information of the selected stations, including the name, station ID, elevation, and the surface temperature at the first pentad (STF), respectively. In order to further investigate the features of SD in different stations, stations are divided into three categories (type A: STF > 5°C; type B: 0°C < STF ≤ 5°C; type C: STF ≤ 0°C). Elevations of the type A stations (TAS) and the type C stations (TCS) are generally below 3850 m and above 4400 m, respectively, while the elevation of type B stations (TBS) is between them, except for the Zuogong station (Table 1).

Figures 2(a) and 2(b) show climatological (1979–2004) pentad mean of surface temperature and SD over the southern TP for the different types of stations from pentad-1 to pentad-18. The surface temperature of the three types of stations shows a linear-like increase with the coming of summer (Figure 2(a)). The SD in TAS is the shallowest in pentad-1 and disappears after pentad-10. The SD in TBS begins to melt gradually after pentad-3 and is less than 0.1 cm after pentad-9. The SD in TCS exhibits the largest standard deviation and fluctuates until about pentad-10. After that, it melts rapidly and almost disappears at pentad-

18 (Figure 2(b)). The abovementioned analysis implies that snow melting firstly occurs in the middle and low elevation areas, after about pentad-10 snow melting over the southern TP mainly appears in the higher elevation, accompanied by the accelerated melting rate.

Figure 2(c) shows climatological pentad mean of SD over the southern TP from satellite-derived data with a decreasing trend from pentad-1 to pentad-18. The snow melting speed is not uniform during the AMJ. To verify this phenomenon, we use the running *t*-test method to the time series of climatological pentad mean of SD to acquire its change point [47]. There is a transition pentad around pentad-10, which is statistically significant at the 99.99% confidence level (Figure 2(d)). Considering that the SD was close to zero in pentad-16, the snow melting period can be divided into two periods: pentad-4 to pentad-9 (P1: April 16th–May 15th) and pentad-10 to pentad-15 (P2: May 16th–June 14th). The averaged pentad change of SD from pentad-4 to pentad-9 (pentad-10 to pentad-15) is −0.21(−0.24) cm/pentad. These results imply that both the satellite-derived and station data demonstrate that snow melting accelerated after about pentad-10.

The snow melts gradually over the southern TP during the period of AMJ, accompanied by the atmospheric warming (Figures 3(a) and 3(b)). Compared with P1, a warming center is located over the Bay of Bengal and accompanied by strong southerlies over the southern TP during P2. At the same time, the apparent heat source is gradually enhanced over the Bay of Bengal and the Indochina Peninsula (Figures 3(c) and 3(d)). The apparent heat source not only shifts the temperature ridgeline at upper-level northward accompanied by the establishment of South Asian high [48] but also causes the air-sea instability that may lead to a spring predictability barrier [49, 50]. In comparison, the diabatic heating is stronger during P2 than P1 over the southern slope of the TP and Indochina Peninsula. The differences of atmospheric temperature between P2 and P1 at different levels are shown in Figure 4, which exhibits a remarkable warming below 200 hPa from P1 to P2. Notably, there is a warming center over the TP at 300–400 hpa (Figures 4(e) and 4(f)). Such a warming may be attributed to the expansion of diabatic heating from the Indochina Peninsula to the Bay of Bengal, which is accompanied by an anticyclone to the south of the TP during the P2 period (Figures 3(b) and 3(d)). The air temperature difference between P2 and P1 reveals a significant warming center located at middle and upper troposphere over the southern Tibetan Plateau. During period P2, the acceleration of snow melting is predominantly observed at higher elevations and can be attributed to an increase in local air temperature.

To further illustrate the difference in temperature changes between the two periods, relative contribution of multiple atmospheric processes to the local temperature change in P1 and P2 is analyzed by the thermodynamic equation (Figure 5). It shows that the local temperature changes over the southern TP at 200–500 hPa during both two periods are slightly positive, but the relative roles of physical processes are different. Diabatic heating and
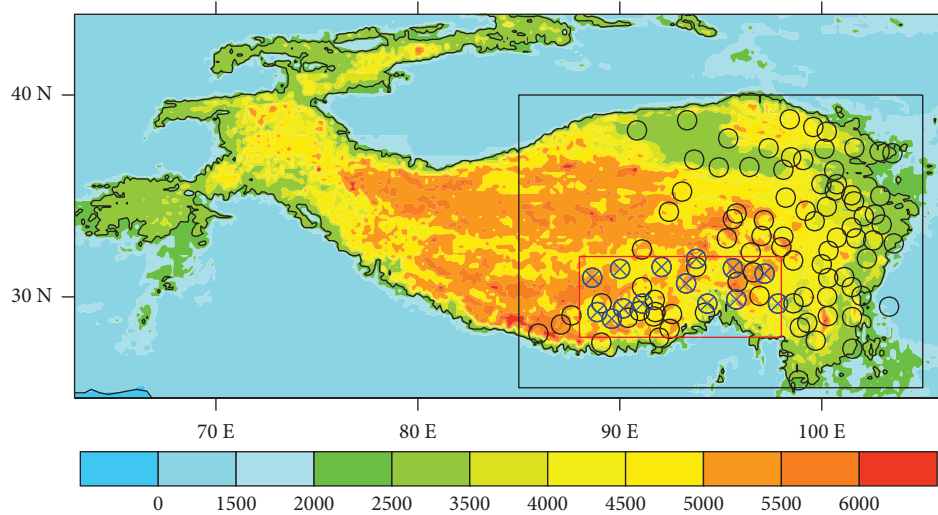
FIGURE 1: Spatial distribution of the meteorological stations (black circle) over the eastern TP (black box: 25.5°N–40°N, 85°E–105°E). The black line represents elevation of 2500 (m). The southern TP domain (28°N–32°N, 88°E–98°E) is outlined by the red box. The blue cross represents stations shown in Table 1.

TABLE 1: Name, station ID, elevation, STF, and types of the 14 CMA stations.

No.	Name	Station ID	Elevation (m)	STF (°C)	Type
1	Naqu	55299	4507	−2.6	C
2	Bange	55279	4700	−2.47	C
3	Jiali	56202	4488.8	−2.07	C
4	Shenza	55472	4672	−2.01	C
5	Suoxian	56106	4022.8	1.15	B
6	Dingqing	56116	3873.1	1.98	B
7	Zuogong	56331	3780	2.97	B
8	Gyantse	55680	4040	4.35	B
9	Nimu	55585	3809.4	6.39	A
10	Shigatse	55578	3836	6.58	A
11	Chamdo	56137	3306	6.7	A
12	Bome	56227	2736	7.2	A
13	Nyingchi	56312	2991.8	7.59	A
14	Lhasa	55591	3648.9	7.83	A

meridional temperature advection contribute to the positive temperature change in the two periods, with larger values in P2 than those in P1 (Figure 5). The warming effect is mainly compensated by the cooling effect of vertical temperature advection in P2 and both vertical temperature advection and zonal temperature advection in P1. The cooling effect of vertical temperature advection in P2 is nearly three times as much as that in P1, while the zonal temperature advection shows a negligible effect in P2 (Figure 5).

3.2. The Interannual Relationship between the Diabatic Heating over South Asia and SD over the Southern TP during Different Snow Melting Periods: Roles of the Air Temperature. Time series of the annual southern TP SD indices during two periods are presented in Figure 6. On the interannual time scale, the correlation of SSDI between the two periods is 0.43, which is significant at the 95% confidence level. This reflects that SD anomalies have high persistence during the two periods. Previous works [17, 18] found that surface

temperature is the main factor affecting SD in spring and summer. Figures 7 and 8 show the correlations of large-scale circulation and air temperature with the SSDI in P1 and P2. During positive SSDI in P1, in the upper troposphere, a negative temperature center is found over the TP and extends to southern China. Correspondingly, there is anomalous cyclonic circulation over the TP, accompanied by anomalous westerly flow over the tropical Indian Ocean and which stretches from the East Africa to the western North Pacific (Figure 7(a)). In the middle troposphere, cold temperature anomaly appears over the southern Bay of Bengal, while warm anomalies are found to the south of Philippines and east of the Iran Plateau. The southern TP is located at the north of the cyclonic anomaly, which is dominated by the anomalous easterlies (Figure 7(c)). The anomalous downward motion is found the southern TP, accompanied by cold air temperature from the surface to 200 hPa (Figure 8(a)). During positive SSDI in two periods, in the upper troposphere, a negative temperature anomaly and anomalous cyclonic circulation appear over the TP, with
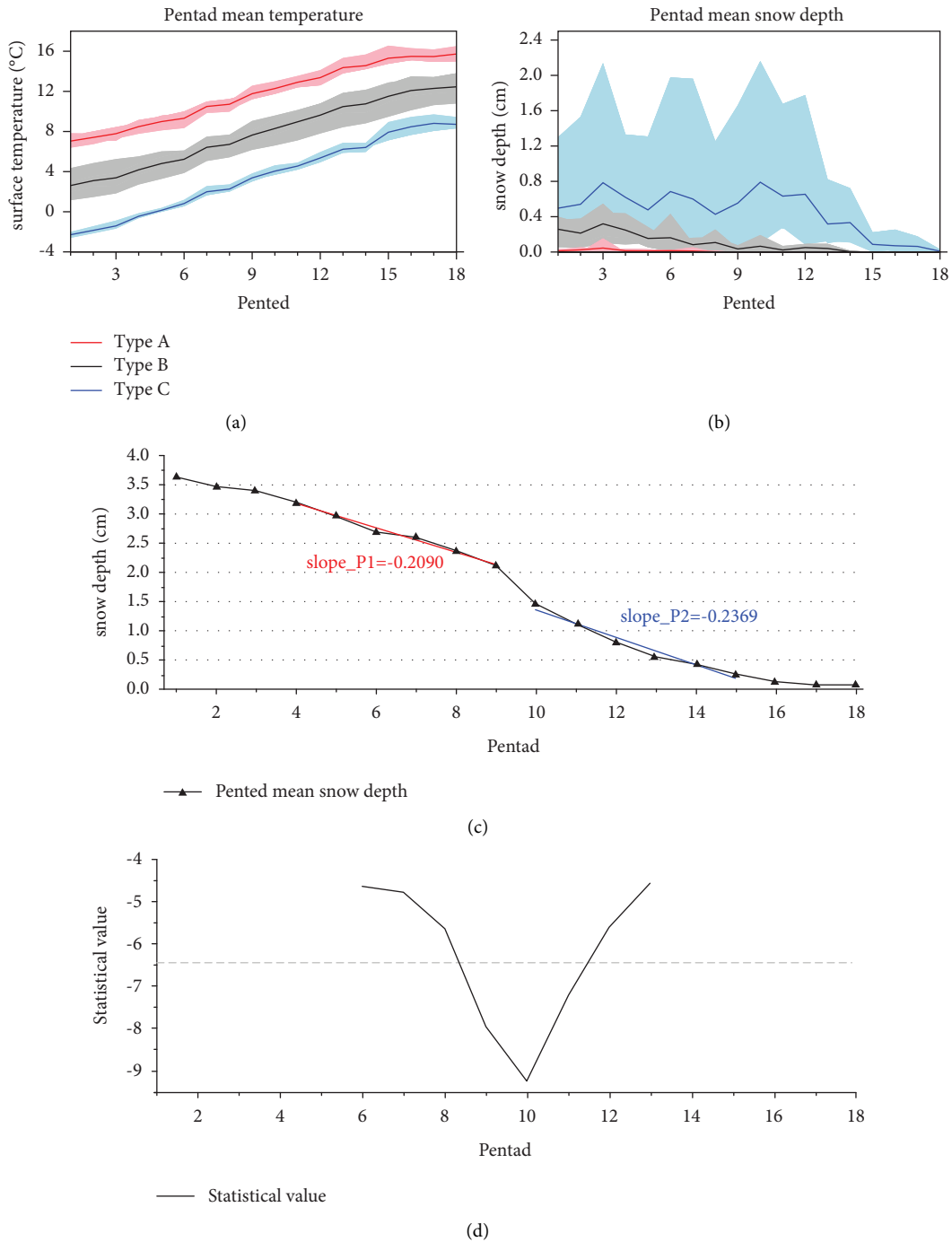
(a)

(b)

(c)

(d)

Figure 2: Climatological (1979–2004) pentad mean evolution of (a) 2 m temperature (°C) and (b) snow depth (cm) over the southern Tibetan Plateau for the different types of stations (shading) and their composites (solid lines) from pentad-1 (1–5th April) to pentad-18 (24–29th June). (c) Climatological pentad mean evolution (cm; black line) of the snow depth over the southern Tibetan Plateau from the satellite-derived snow depth data. (d) The result of 11-pentad running t-test method. The dashed lines represent the critical values at the 99.99% significance level. In (a) and (b), the red line denotes the composite result for type A stations, the black line denotes the composite result for type B stations, and the blue line denotes the composite result for type C stations.

their center located slightly northward in P2 (Figures 7(a) and 7(b)). Compared with the positive SSDI in P1, in the middle troposphere, the cold center over the southern TP is weaker in P2 and the anomalous cyclonic circulation to the east of the TP associated with the anomalous northerlies

over the TP (Figure 7(d)). Similar to the positive SSDI in P1, negative temperature centers appear over the TP at 400–200 hPa in P2 (Figure 8(b)). These characteristics further illustrate the close relationship between SD over the southern TP and local air temperature [17, 18].
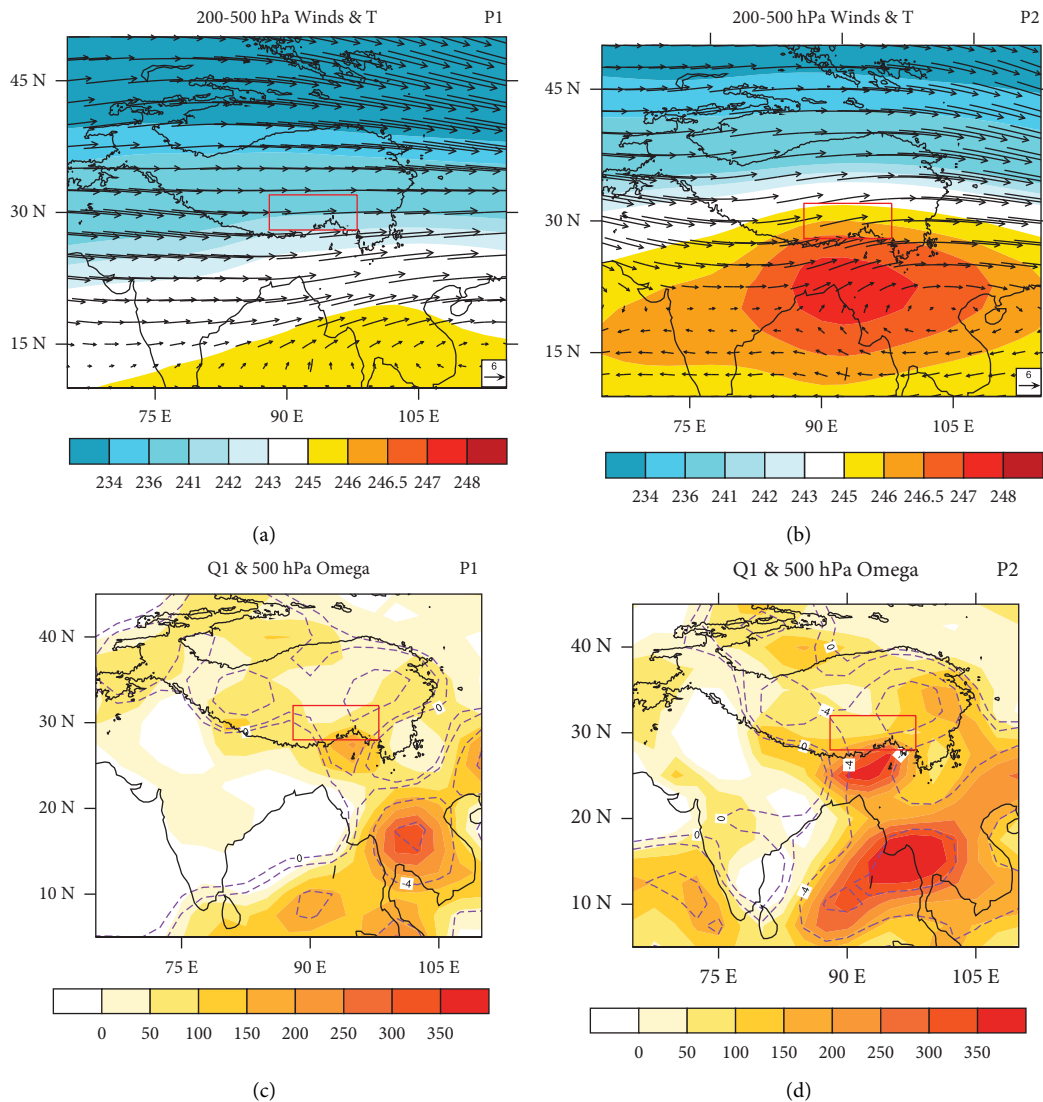
(a)

(b)

(c)

(d)

FIGURE 3: Spatial patterns of the atmospheric mean state in the two periods. Climatological mean 200–500 hPa winds (vector, m/s) and temperature (shading, (K) in (a) P1 and (b) P2). Climatological mean Q1 (shading, W/m2) and 500 hPa Omega (dotted lines denote negative values, 102 Pascal/s) in (c) P1 and (d) P2.

The diabatic heating over the South Asian monsoon region is one of the important factors to modulate air temperature over the TP [51]. In order to illustrate the role of the diabatic heating anomalies over South Asia in the year-to-year variability of SD over the southern TP, Figure 9 shows the correlations of Q1 with the SSDI in P1 and P2. During P1, the significant negative correlations are located from the Bay of Bengal eastward to the western South China Sea (Figure 9(a)). In comparison, the significant negative (positive) correlation is located over the northern Indochina Peninsula (southern China) during P2 (Figure 9(b)). Here, we propose three indices: one is defined as Q1 anomalies averaged over the region (8°–13°N, 90°–110°E) in P1 (Q1P1), the second is defined as Q1 anomalies averaged over the northern Indochina Peninsula (15°–20°N, 100°–108°E) in P2 (Q1IPP2), and the last one is defined as Q1 anomalies averaged over southern China (23°–27°N, 108°–115°E) in P2

(Q1SCP2). The time series of the abovementioned Q1 indices in two periods is shown in Figure 6. In P1, the correlation coefficient between SSDI and Q1P1 is −0.74. In P2, the correlation coefficient between SSDI and Q1IPP2 (Q1SCP2) is −0.49 (0.49). All the correlation coefficients are significant at the 99% confidence level.

To further investigate how diabatic heating over different areas leads to anomalous SD over the southern TP in the two periods by affecting local air temperature, the large-scale circulation and air temperature related to the three Q1 indices are calculated (Figures 10 and 11). During the negative years of Q1P1 in P1, there is a cyclone anomaly and anomalous cold air temperature center at 200 hPa over the TP, accompanied by a weakened jet stream over the Indian Ocean (Figure 10(a)). In the middle troposphere, cold temperature anomaly is centered to the south of the TP (Figure 10(b)). This pattern bears a large resemblance to the
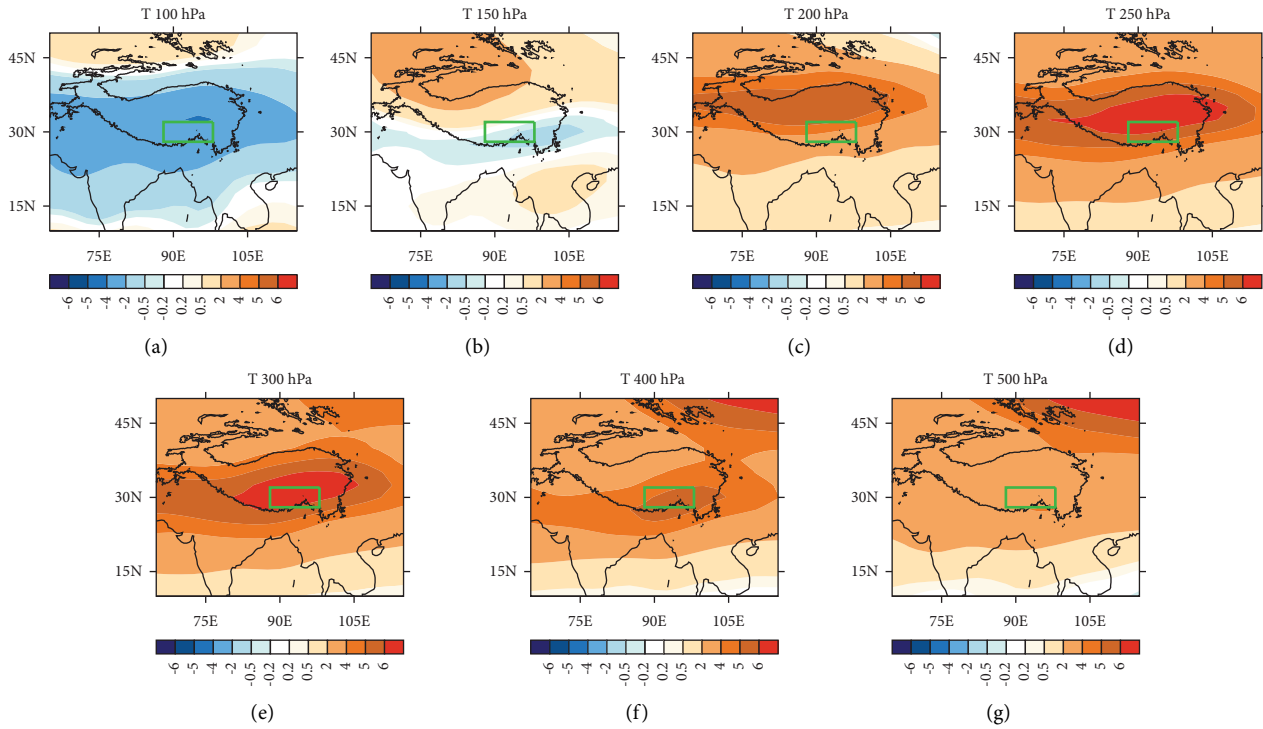
FIGURE 4: Differences of air temperature (shading, (K) at 100 hPa (a), 150 hPa (b), 200 hPa (c), 250 hPa (d), 300 hPa (e), 400 hPa (f), and 500 hPa (g) between P2 and P1).
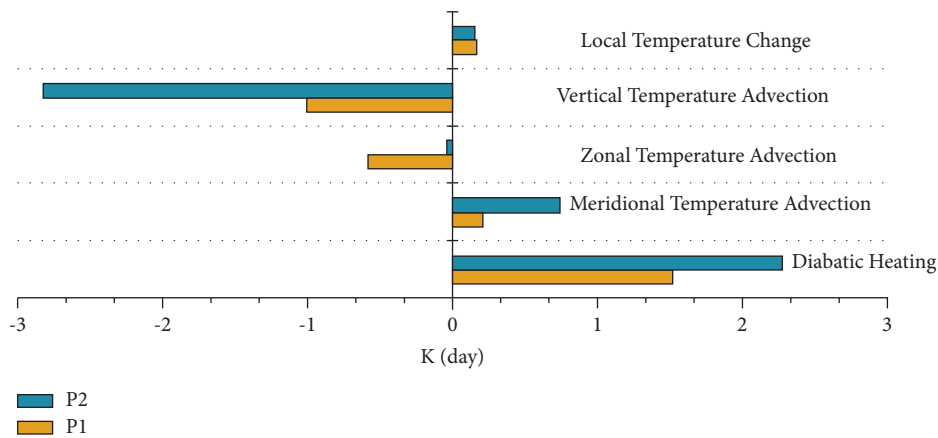

FIGURE 5: Climate mean of the local temperature variation (K/day), vertical temperature advection (K/day), horizontal temperature advection (K/day), and diabatic heating (K/day) at 200–500 hPa in the thermodynamic equation during P1 (dark yellow) and P2 (light blue).

spatial structure of positive SSDI in P1 (Figures 7(a) and 7(c)). In addition, the linear correlation coefficient between the Q1P1 and SSDI is −0.74, significantly exceeding the 99.9% confidence level. The abovementioned results indicate that Q1P1 may be one of the key factors affecting SSDI in P1. It seems that the suppressed diabatic heating from the Bay of Bengal eastward to the western South China Sea could induce an anomalous cyclone at the upper-level and downward motions over the TP through the Gill model response, leading to cold air temperature from the surface to 200 hPa (Figures 10(a), 10(b) and 11(a)) and hence above-normal SD over the southern TP. In P2, during the negative years of

Q1IPP2, the cold air temperature center and cyclone anomalies appear over the western TP at 200 hPa (Figure 10(c)). From the pressure-latitude cross-section of the air temperature and circulation averaged over (85°N–100°N), the anomalous downward motion and cold air temperature center at about 300 hPa are observed on the southern TP slope related to diabatic cooling over the northern Indochina Peninsula (Figure 11(b)). During positive years of Q1SCP2, there are two cold centers located on the TP and the Korean Peninsula at 200 hPa (Figure 10(e)). The pressure-latitude cross-section of air temperature associated with the positive Q1SCP2 years is similar to those
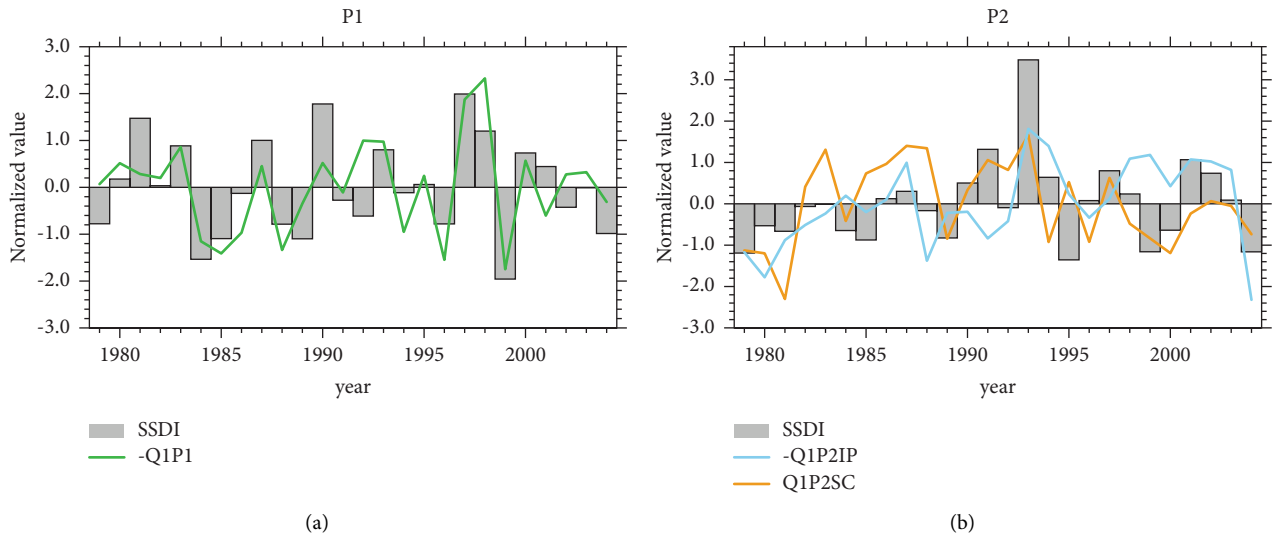
(a)

(b)

FIGURE 6: The time series of normalized SSDI and Q1P1 indices during P1 (a) and normalized SSDI, Q1IPP2, and Q1SCP2 during P2. (b) The gray columnar denotes the SSDI, and the green, light blue, and orange lines denote the QIP1, Q1IPP2, and Q1SCP2, respectively.
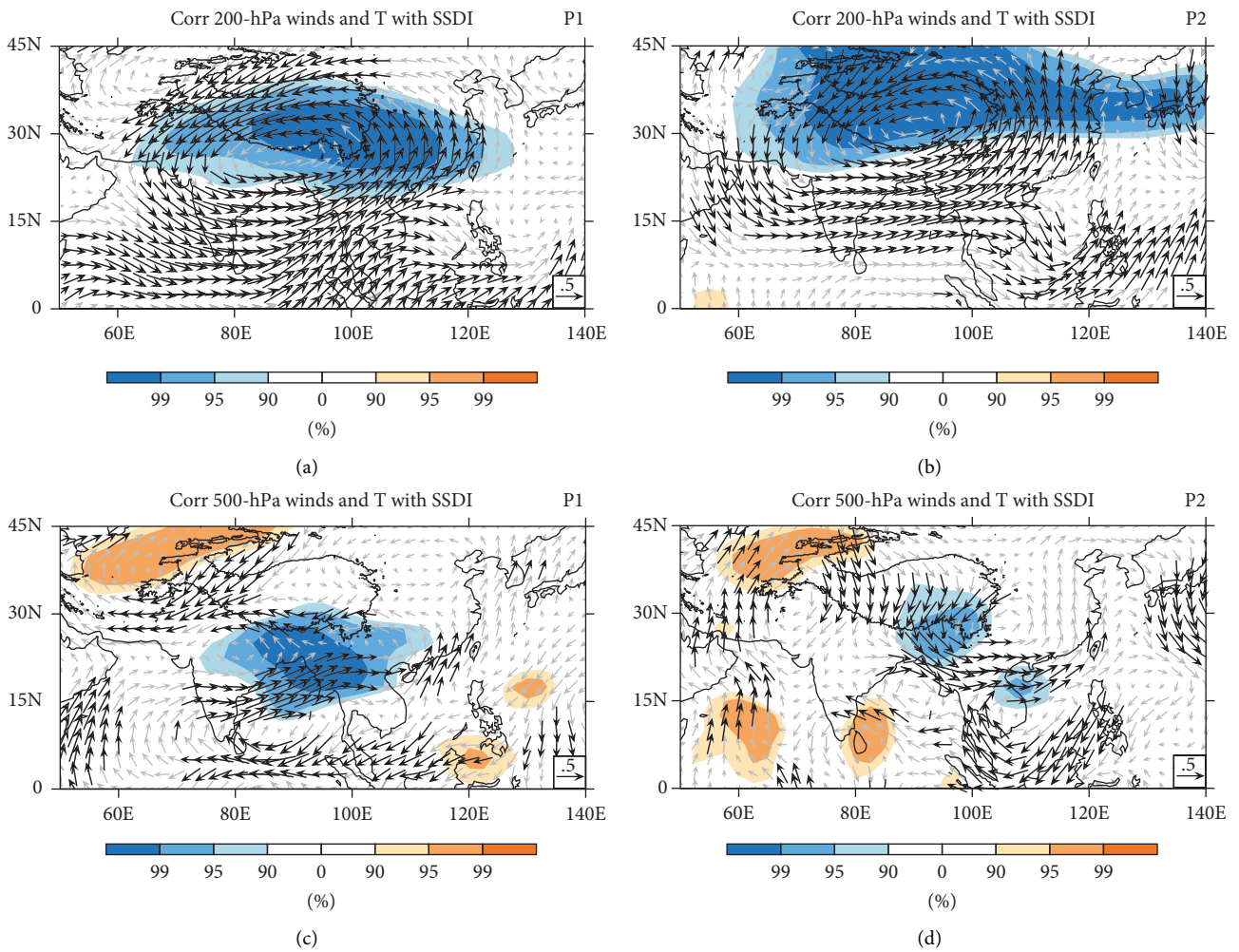

(a)

(b)

(c)

(d)

FIGURE 7: At 200 hPa (a, b) and 500 hPa (c, d), correlations of wind (vector) and air temperature (shading) with the SSDI in P1 (a, c) and P2 (b, d) for 1979–2004, respectively. The black vectors indicate winds exceeding the 90% confidence level. Shading areas indicate values exceeding the 90%, 95%, and 99% confidence levels.
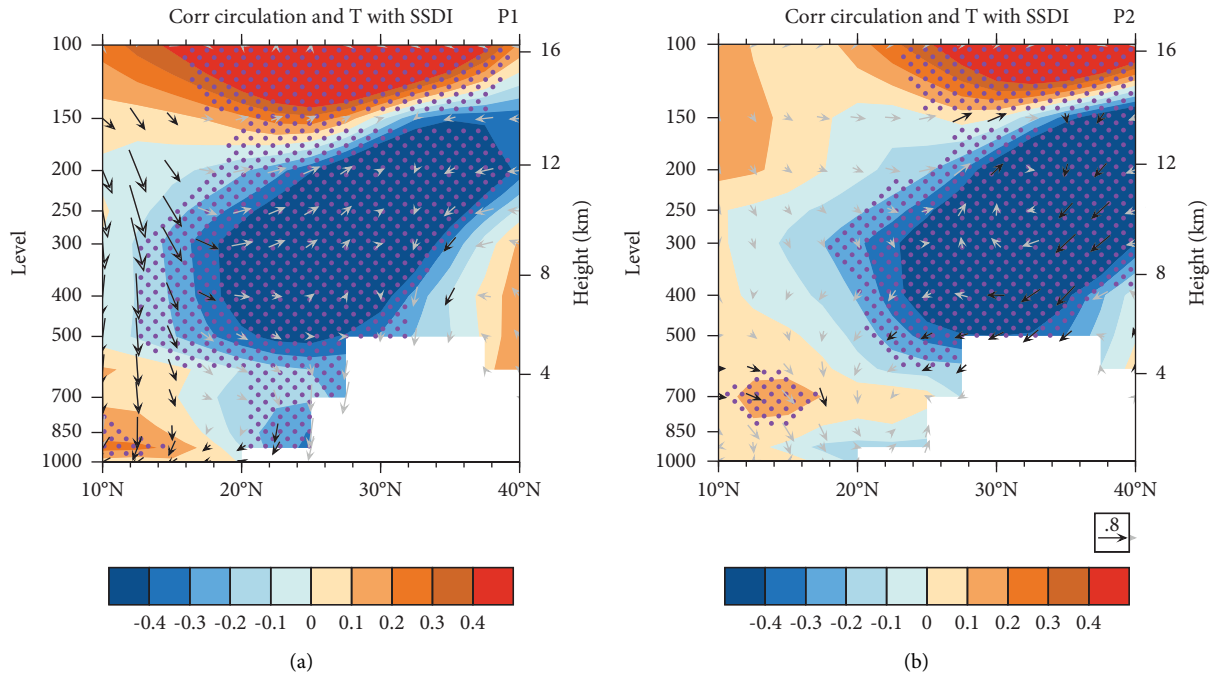
FIGURE 8: Correlations of pressure-latitude cross-section of circulation (vector) and air temperature (shading) averaged over (88°E–98°E) with the SSDI in P1 (a) and P2 (b), respectively. The black vectors and dotted areas indicate values exceeding the 90% confidence level.
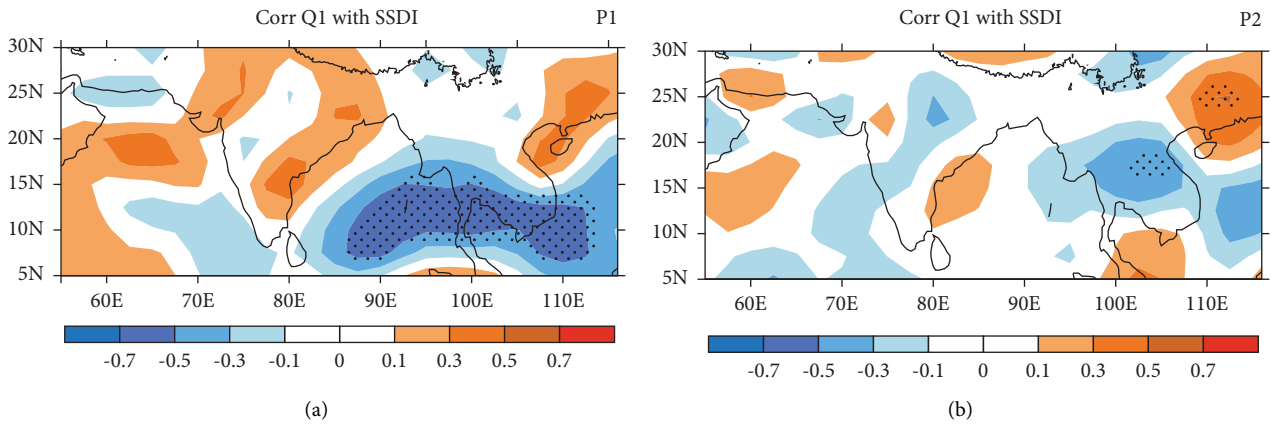

FIGURE 9: Correlation of Q1 with the SSDI in P1 (a) and P2 (b) for 1979–2004. Dotted areas indicate values exceeding the 99% confidence level.

associated with the negative Q1IPP2 years (Figures 11(b) and 11(c)). However, the anomalous cold air temperature associated with diabatic cooling over the northern Indochina Peninsula and diabatic heating over the southern China could not extend from the upper level to the land surface over the southern TP (Figures 10(d), 10(f), and 11(b) and 11(c)).

It is difficult for observational data-based statistical methods to distinguish the individual impact of Q1 over the three regions on the southern TP air temperature in different periods. Thus, a nonlinear baroclinic model is conducted to simulate the atmospheric circulation and temperature anomalies in response to the individual Q1 anomalies over the three regions during their

corresponding period. Following previous works [11], a heating profile was utilized in the vertical direction to simulate the heating anomalies, with the maximum located at sigma 0.37 (Figure 12(a)). The horizontal structure and magnitude of heating depend on the regressions of Q1 against SSDI during two periods. This involves conducting separate regressions for each period. The idealized heating is presented as $Q = V(\sigma) A(\lambda, \phi)$. The vertical structure of heating is showed $V(\sigma)$. The function $A(\lambda, \phi)$ represents the horizontal structure and magnitude of heating [11]. The maximum value of the heating rate equals the five times value of the regression coefficient of Q1 which is significant exceeding the 80% confidence level. Four experiments are conducted as
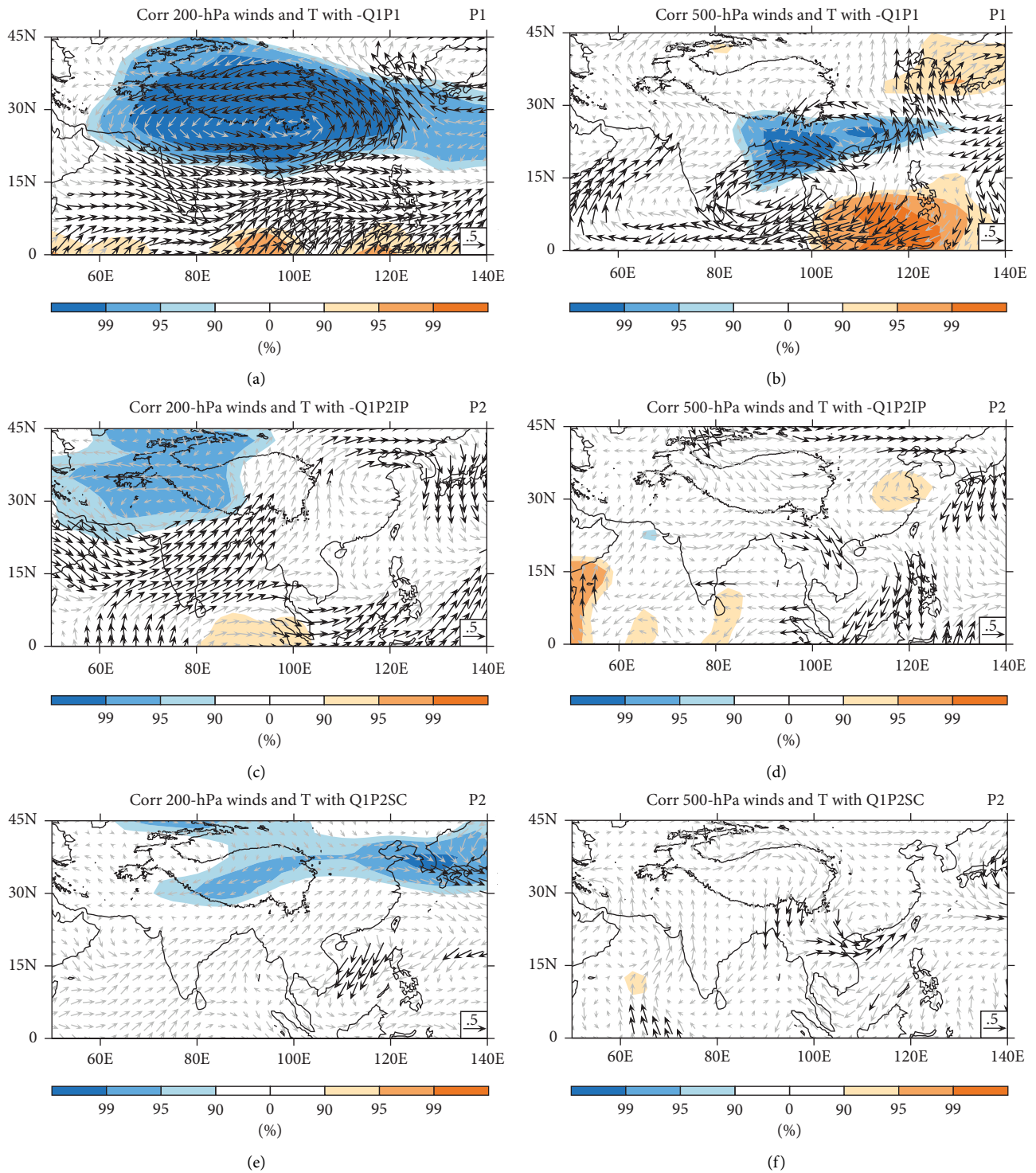
FIGURE 10: At 200 hPa (a, c, e) and 500 hPa (b, d, f), correlations of wind (vector) and air temperature (shading) with the (a, b) negative Q1P1 in P1, (c, d) negative Q1IPP2, and (e, f) Q1SCP2 in P2 for 1979–2004, respectively. The black vectors indicate winds exceeding the 90% confidence level. Shading areas indicate values exceeding the 90%, 95%, and 99% confidence levels.

follows: during P1, (1) heating is added from the Bay of Bengal eastward to the western South China Sea; (2) during P2, heating is added over the regions of the northern Indochina Peninsula and the southern China;

(3) the regions of the northern Indochina Peninsula; (4) the regions of the southern China. Figures 12(b) and 12(c) show the horizontal magnitude and structure of the heating process at sigma of 0.37 in the three regions.
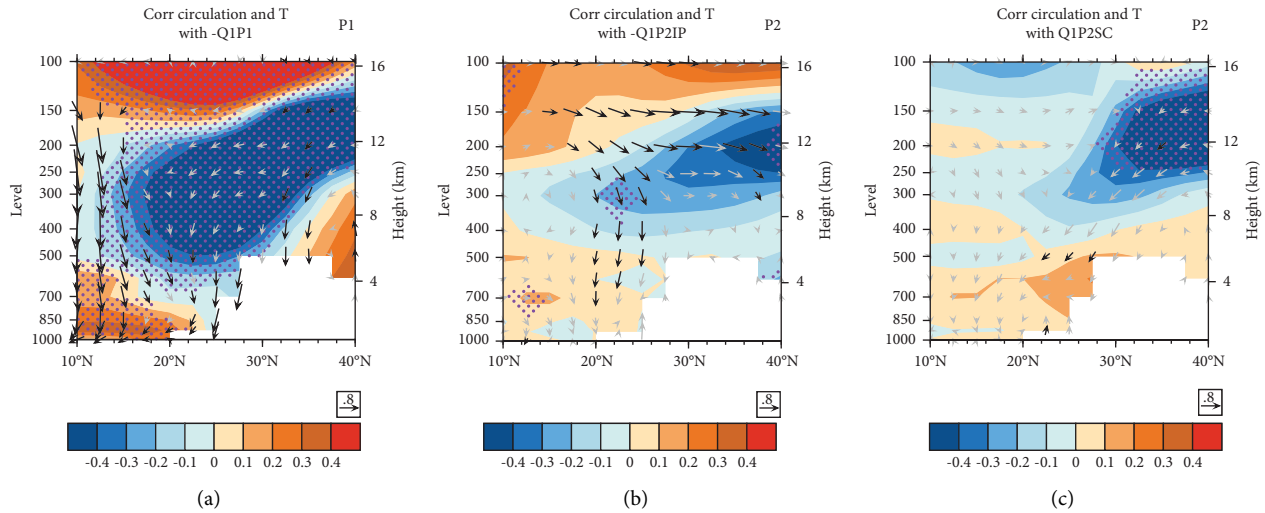
FIGURE 11: Correlations of pressure-latitude cross-section of circulation (vector) and air temperature (shading) averaged over (85°E–100°E) with the (a) negative Q1P1 in P1 and with (b) negative Q1IPP2 and (c) Q1SCP2 in P2, respectively. The black vectors and dotted areas indicate values exceeding the 90% confidence level.
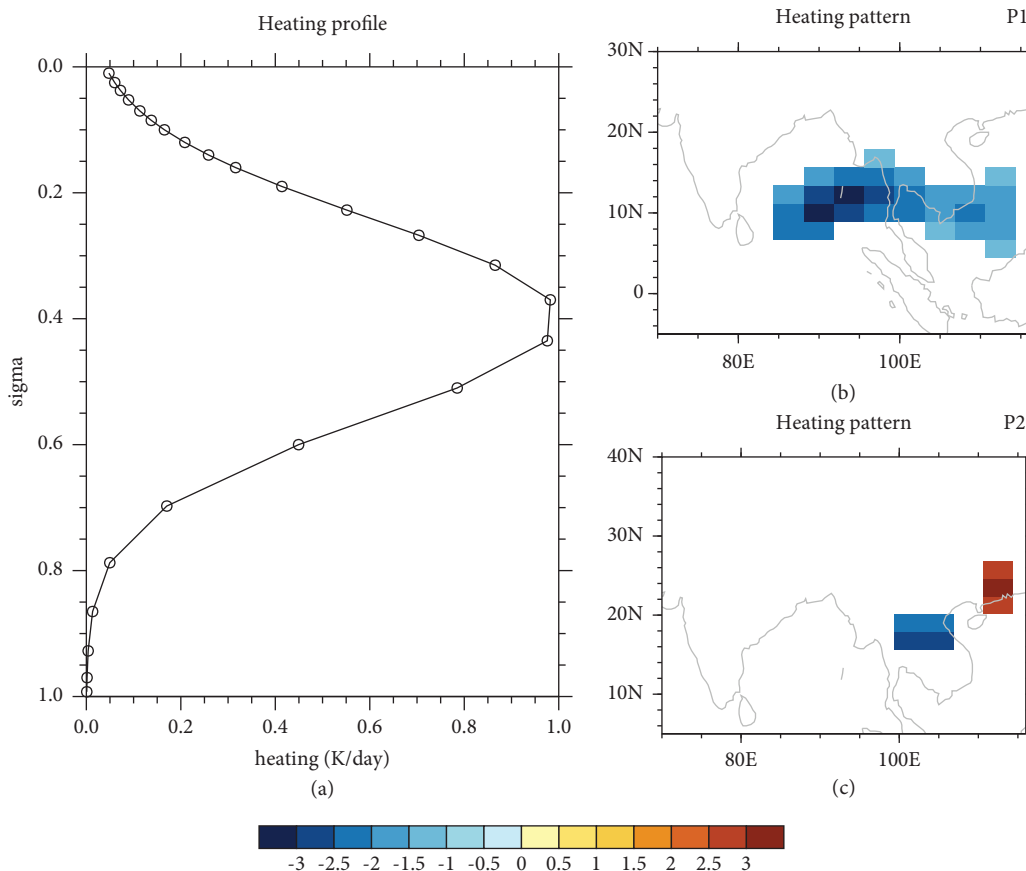

FIGURE 12: (a) The vertical profile of the specific heat source (K/day). The x-axis and y-axis in (a) denote the magnitude of the heating process and height represented by sigma, respectively. The spatial pattern of specific heat sources (shading; K/day) at the level of sigma that equals 0.37 during P1 (b) and P2 (c).

The response of air temperature and atmospheric circulation in different heating experiments are presented in Figures 13–15. In response to cooling from the Bay of Bengal eastward to the western South China Sea, an upper-level cyclone appears over the region of (0–30°N, 50–110°E) in P1, consistent with the correlation pattern for the negative Q1P1
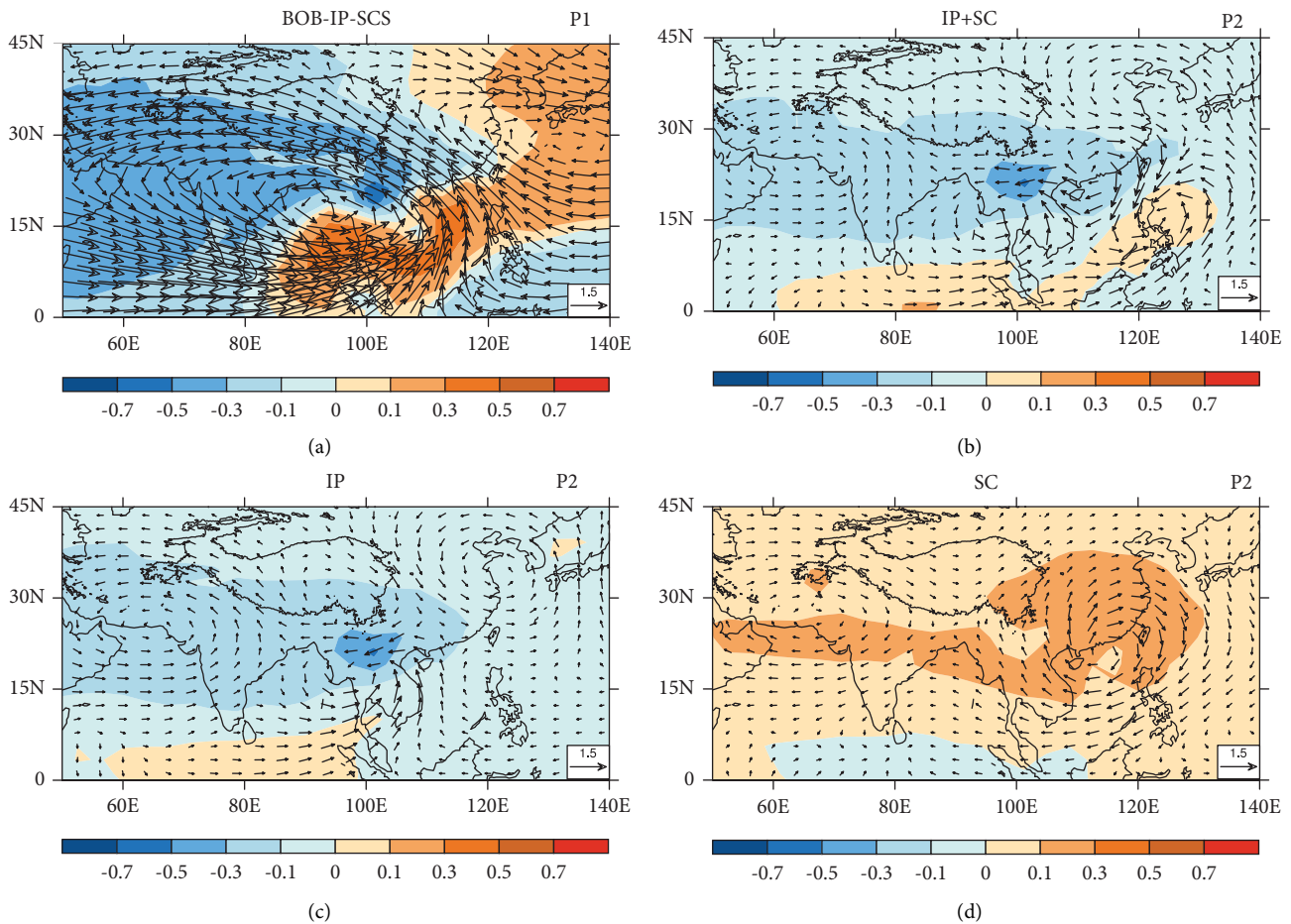
FIGURE 13: The responses of winds (m/s) and air temperature (K) at 200 hPa to heating over the southern Bay of Bengal to the western South China Sea (BOB-IP-SCS) (a) in P1. Same as in (a) but for responses to heating over the northern Indochina Peninsula (IP) and southern China (SC) (b) IP (c) and SC (d) in P2.

and positive SSDI, but it exhibits a more southward center (Figures 7(a), 10(a), and 13(a)). The warm and cold air temperature anomalies appear over the southeastern and northwestern portion of the cyclone (Figure 13(a)). Similarly, their downward motions and cold air temperature over the southern TP are consistent with the observational results (Figures 11(a) and 15(a)). Indeed, the cold atmospheric temperature at the lower or surface layer (Figures 14(a) and 15(a)) on the southern TP slope is conducive to deepening of SD over the southern TP.

In P2, the cooling forcing over the northern Indochina Peninsula excites a pair of cyclonic circulation over its northeastern and southern flanks (Figure 13(c)). The cyclonic circulation anomaly over western TP in response to the diabatic cooling over IP in the experiment is much weaker and located southeastward compared to that in observation (Figures 10(c) and 13(c)). There is anomalous anticyclonic circulation and warm temperature anomaly over the Indochina Peninsula at 500 hPa (Figure 14(c)). Correspondingly, the cold air temperature center appears to the south of TP at the tropopause (250–400 hPa) and did not extend to the land surface over the southern TP (Figure 15(c)). Nevertheless, the anomalous upper-level

cooling and downward motions around the TP are similar to those in the observation (Figures 11(b) and 15(c)). In contrast, heating over the southern China could increase air temperature in most areas of the TP, implying that the results in the model experiment are not consistent with the statistical analysis in observation (Figures 10(e), 10(f), 11(c), 13(d), 14(d), and 15(d)). Combined forcing types over the two regions induce patterns similar to that over the northern Indochina Peninsula (Figures 13(b), 13(c), 14(b), 14(c), 15(b), and 15(c)), implying that cooling over the northern Indochina Peninsula contributed largely to temperature and circulation changes induced by the combined forcing types.

In conclusion, the abovementioned results suggest that anomalous diabatic heating from the Bay of Bengal eastward to the western South China Sea could significantly affect the SD variation over southern TP by modulating local surface air temperature during P1. On the other hand, both Q1P2IP and Q1P2SC have a significant relationship with the SD over the southern TP during P2 in observation. But neither cooling over the Indochina Peninsula nor heating over southern China can directly affect surface temperature over the southern TP.
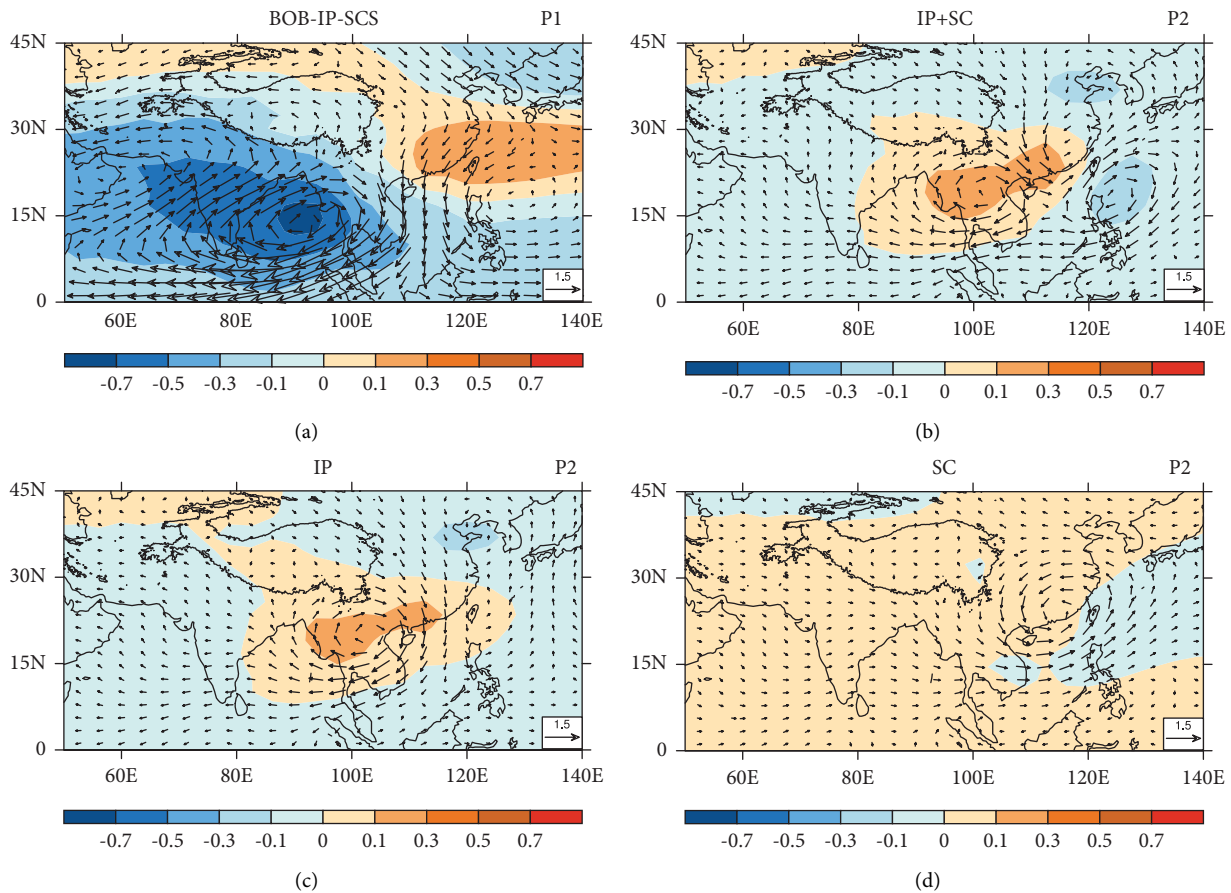
Figure 14: As in Figure 13, but at 500 hPa.

4. Discussion

In P2, the diabatic cooling over the northern Indochina Peninsula leads to an anomalous cyclone at 200 hPa over the western TP and downward motions over the southern TP slope, accompanied by negative temperature anomalies at the midhigh levels. This midhigh level anomalous cold temperature may be conducive to deepening of SD over the southern TP, providing that snow melting is mostly observed at high elevations during P2. However, more reliable and high resolution data are needed to further identify the results. The current study could not provide convincing evidence that diabatic cooling over the northern Indochina Peninsula has a significant impact on the southern TP SD by modulating the surface temperature in P2. The diabatic heating over southern China is associated with the cold-than-normal air temperature at the upper level over the TP during P2 in observation, but the experiments with a nonlinear baroclinic model did not demonstrate the decrease of air temperature over the TP in response to the diabatic heating over southern China. In terms of climate states, diabatic heating over the southern TP contributes larger to the local positive temperature change in P2 than that in P1 (Figure 5(a)). However, the simple model ignores feedback of convection [37]. Given that the baroclinic model is a dry mode,

an anomalous vertical motion during the P2 period may induce a local temperature change without corresponding abnormal latent heating. Such errors have the potential to magnify during the P2 period and ultimately influence the model results. Therefore, it should pay attention to the applicability of the simple model in different periods when simulating the changes in air temperature over the southern TP.

As global warming stoppage around 2000 and the limited number of quality control stations over southern TP, to avoid contamination of the results by these, the time period 1979–2004 is used. Nevertheless, to use the satellite-derived data during 1979–2020, climatological pentad mean of southern TP SD (figure not shown) was the same as in Figures 2(c) and 2(d). These also imply that southern TP SD can be divided into two periods. Recently, ice losses at high elevations have also received increased attention in the context of global warming [52]. More high quality monitoring of SD and snow cover data over the TP need to be carried out, especially at high elevations. In addition, the effect of human action cannot be ignored, for example, the role of absorbent aerosols over TP in different snowmelt stages. Whether there is interdecadal variation in the southern TP SD during the two periods in recent years deserves further study.
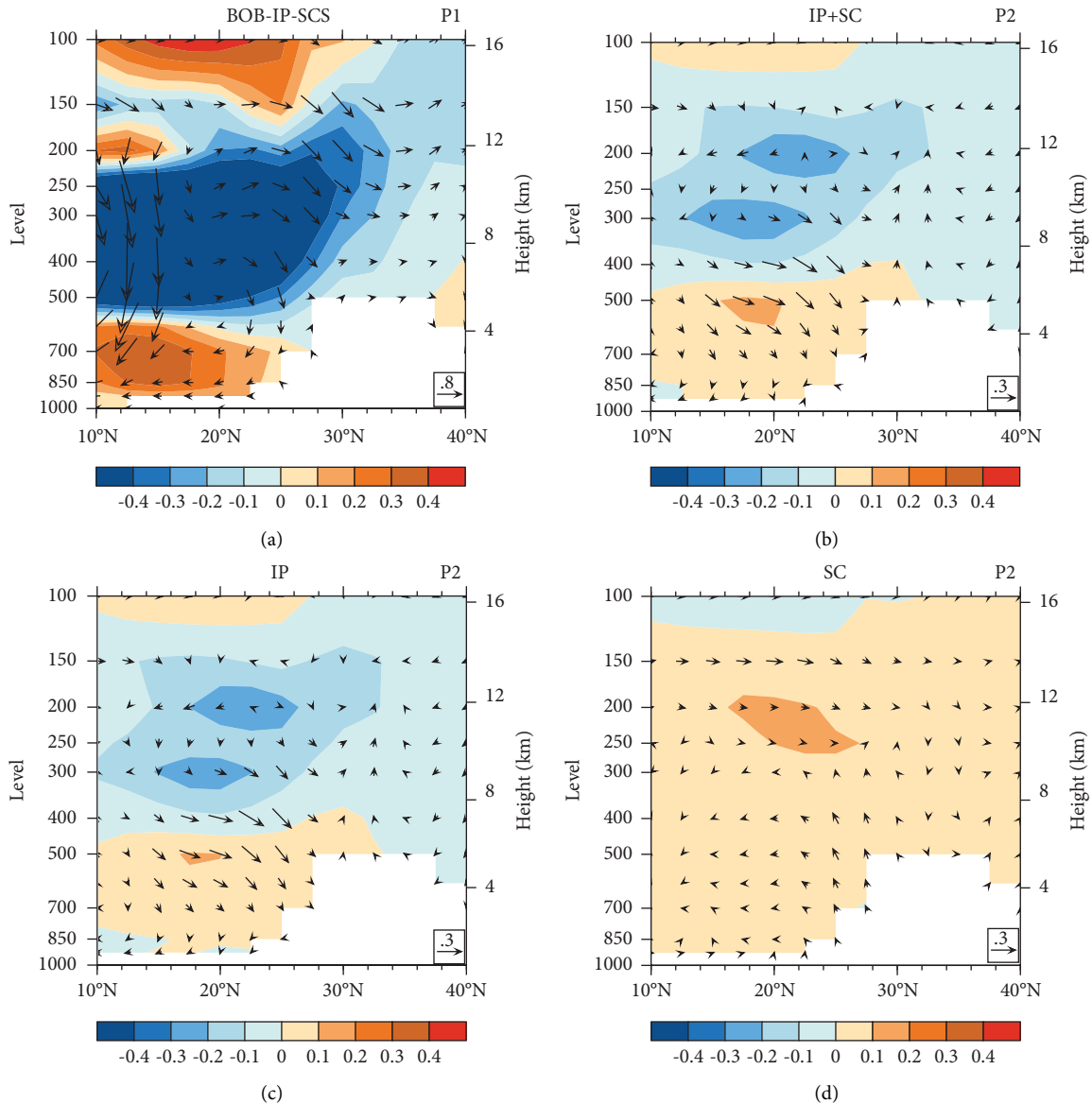
Figure 15: The responses of pressure-latitude cross-section of circulation s (meridional vector, m/s; vertical velocity, 5×10^{-6} Pascal/s) and air temperature (K) anomalies averaged over (85°E–100°E) to heating over BOB-IP-SCS in P1 (a) Same as in (a) but for responses to heating over northern IP and SC (b), northern IP (c), and SC (d) in P2.

5. Conclusions

During the spring-summer transitional season, the concentrated area of snow cover is located over southern TP slope, which is closely related to the weather and climate in Asia. Understanding the characteristics of snowmelt and its associated mechanisms over the TP during the transition season is critical for the regional water cycle research. From the in situ observational results, the previous work [18] found that unlike in other areas of central and eastern TP, snow over the southern TP slope could have almost completely melted in summer. Compared to snowfall, surface temperature changes are the main factors affecting SD variations during spring and summer. This study investigates the climatic characteristics and interannual variation of snow depth over the southern Tibetan Plateau during late spring to early summer, with

a focus on local air temperature. Our analysis is based on various observational data sources for snow depth over TP, NCEP/NCAR reanalysis data, as well as experiments conducted using a nonlinear baroclinic model. The main results are summarized as follows:

(1) From the perspective of climate states, according to the characteristics of SD evolution from station data and improved satellite-derived data, the transition period of spring-summer is further divided into two periods (P1: April 16th–May 15th and P2: May 16th–June 14th). The snow melting rate in P2 is faster than that in P1. This melting acceleration mainly comes from high elevations.

(2) Difference of air temperature between P2 and P1 shows a remarkable warming center at about 300 hPa

over the southern TP. Diagnoses of the thermodynamic equation further demonstrate that the local temperature changes over the southern TP at 200–500 hPa during both the periods are slightly positive and the warming over southern TP during the two periods is mainly attributed to the meridional temperature advection and diabatic heating in situ.

(3) On the interannual time scale, from the surface to 200 hPa, corresponding to deepening of SD over the southern TP, cold air temperature is observed over the TP in the two periods.

(4) In P1, the diabatic cooling from the southern Bay of Bengal eastward to the western South China Sea induces an anomalous cyclone at 200 hPa over the TP and downward motions over the southern TP and Bay of Bengal, leading to cold air temperature anomalies from surface to 200 hPa over the southern TP. The lower-than-normal temperature provided favorable conditions for the above-normal SD.

(5) In P2, the variation of SD over the southern TP is strongly linked to diabatic cooling over the northern Indochina Peninsula and diabatic heating over southern China.

An earlier version of the manuscript Zhang et al. [53] has been published as a "Preprint" in research square.

Data Availability

The reanalysis data in this paper are downloaded from NCEP–NCAR (https://www.esrl.noaa.gov/psd/data/gridded/data.ncep.reanalysis.html). The satellite-derived data are downloaded from TPDC (https://data.tpdc.ac.cn/zh-hans/data/df40346a-0202-4ed2-bb07-b65dfcda9368/). The in situ observations are obtained via the China Meteorological Administration National Meteorological Information Centre (https://data.cma.cn/en).

Conflicts of Interest

The authors declare that they have no conflicts of interest.

Acknowledgments

References

[1] X. Cui, H. Graf, B. Langmann, W. Chen, and R. Huang, "Hydrological impacts of deforestation on the southeast Tibetan plateau," *Earth Interactions*, vol. 11, no. 15, pp. 1–18, 2007.

[2] G. Wu, Y. Liu, Q. Zhang et al., "The influence of mechanical and thermal forcing by the Tibetan Plateau on Asian climate," *Journal of Hydrometeorology*, vol. 8, no. 4, pp. 770–789, 2007.

[3] K. Yang, B. Ye, D. Zhou et al., "Response of hydrological cycle to recent climate changes in the Tibetan Plateau," *Climatic Change*, vol. 109, no. 3-4, pp. 517–534, 2011.

[4] A. Duan, G. Wu, Y. Liu, Y. Ma, and P. Zhao, "Weather and climate effects of the Tibetan Plateau," *Advances in Atmospheric Sciences*, vol. 29, no. 5, pp. 978–992, 2012.

[5] G. Jeelani, J. J. Feddema, C. J. van der Veen, and L. Stearns, "Role of snow and glacier melt in controlling river hydrology in Liddar watershed (western Himalaya) under current and future climate," *Water Resources Research*, vol. 48, no. 12, Article ID 12508, 2012.

[6] H. C. Ren, W. Li, H. L. Ren, and J. Zuo, "Distinct linkage between winter Tibetan Plateau snow depth and early summer Philippine Sea anomalous anticyclone," *Atmospheric Science Letters*, vol. 17, no. 3, pp. 223–229, 2016.

[7] T. Wang, Y. Zhao, C. Xu et al., "Atmospheric dynamic constraints on Tibetan Plateau freshwater under Paris climate targets," *Nature Climate Change*, vol. 11, no. 3, pp. 219–225, 2021.

[8] Z. Pu, L. Xu, and V. V. Salomonson, "Modis/terra observed seasonal variations of snow cover over the Tibetan plateau," *Geophysical Research Letters*, vol. 34, no. 6, p. 6706, 2007.

[9] C. Yuan, T. Tozuka, T. Miyasaka, and T. Yamagata, "Respective influences of IOD and ENSO on the Tibetan snow cover in early winter," *Climate Dynamics*, vol. 33, no. 4, pp. 509–520, 2009.

[10] Z. Xiao, A. Duan, and Z. Wang, "Atmospheric heat sinks over the western Tibetan Plateau associated with snow depth in late spring," *International Journal of Climatology*, vol. 39, no. 13, pp. 5170–5180, 2019.

[11] X. Jiang, T. Zhang, C. Y. Tam et al., "Impacts of ENSO and IOD on snow depth over the Tibetan Plateau: roles of convections over the western north Pacific and Indian Ocean," *Journal of Geophysical Research-atmospheres*, vol. 124, no. 22, pp. 11961–11975, 2019.

[12] T. Yasunari, A. Kitoh, and T. Tokioka, "Local and remote responses to excessive snow mass over Eurasia appearing in the northern spring and summer climate," *Journal of the Meteorological Society of Japan*, vol. 69, no. 4, pp. 473–487, 1991.

[13] I. Rangwala, J. R. Miller, G. L. Russell, and M. Xu, "Using a global climate model to evaluate the influences of water vapor, snow cover and atmospheric aerosol on warming in the Tibetan Plateau during the twenty-first century," *Climate Dynamics*, vol. 34, no. 6, pp. 859–872, 2010.

[14] K. Souma and Y. Wang, "A comparison between the effects of snow albedo and infiltration of melting water of Eurasian snow on East Asian summer monsoon rainfall," *Journal of Geophysical Research*, vol. 115, no. 2, p. 2115, 2010.

[15] K. H. Usha, V. S. Nair, and S. S. Babu, "Modeling of aerosol induced snow albedo feedbacks over the Himalayas and its implications on regional climate," *Climate Dynamics*, vol. 54, no. 9-10, pp. 4191–4210, 2020.

[16] P. Zhao, Z. Zhou, and J. Liu, "Variability of Tibetan spring snow and its associations with the hemispheric extratropical circulation and east Asian summer monsoon rainfall: an observational investigation," *Journal of Climate*, vol. 20, no. 15, pp. 3942–3955, 2007.

[17] Z. Xiao and A. Duan, "Impacts of Tibetan Plateau snow cover on the interannual variability of the East Asian summer monsoon," *Journal of Climate*, vol. 29, no. 23, pp. 8495–8514, 2016.

[18] W. Xu, L. Ma, M. Ma, H. Zhang, and W. Yuan, "Spatial–temporal variability of snow cover and depth in the Qinghai–Tibetan Plateau," *Journal of Climate*, vol. 30, no. 4, pp. 1521–1533, 2017.

[19] Z. Wang, R. Wu, and G. Huang, "Low-frequency snow changes over the Tibetan Plateau," *International Journal of Climatology*, vol. 38, no. 2, pp. 949–963, 2017.

[20] K. Gao, A. Duan, and D. Chen, "Interdecadal summer warming of the Tibetan Plateau potentially regulated by a sea surface temperature anomaly in the Labrador Sea," *International Journal of Climatology*, vol. 41, no. 1, pp. E2633–E2643, 2020.

[21] Z. Wang, R. Wu, P. Zhao, S. Yao, and X. Jia, "Formation of snow cover anomalies over the Tibetan Plateau in cold seasons," *Journal of Geophysical Research, [Atmospheres]*, vol. 124, no. 9, pp. 4873–4890, 2019.

[22] R. Senan, Y. J. Orsolini, A. Weisheimer et al., "Impact of springtime Himalayan-Tibetan Plateau snowpack on the onset of the Indian summer monsoon in coupled seasonal forecasts," *Climate Dynamics*, vol. 47, no. 9-10, pp. 2709–2725, 2016.

[23] K. Lau and S. Yang, "Climatology and interannual variability of the Southeast Asian summer monsoon," *Advances in Atmospheric Sciences*, vol. 14, no. 2, pp. 141–162, 1997.

[24] G. Wu and Y. Zhang, "Tibetan plateau forcing and the timing of the monsoon onset over South Asia and the South China sea," *Monthly Weather Review*, vol. 126, no. 4, pp. 913–927, 1998.

[25] B. Liu, Y. Liu, G. Wu, J. Yan, J. He, and S. Ren, "Asian summer monsoon onset barrier and its formation mechanism," *Climate Dynamics*, vol. 45, no. 3-4, pp. 711–726, 2015.

[26] Y. Liu, G. Wu, H. Liu, and P. Liu, "Condensation heating of the Asian summer monsoon and the subtropical anticyclone in the Eastern Hemisphere," *Climate Dynamics*, vol. 17, no. 4, pp. 327–338, 2001.

[27] S. Yang and P. Webster, "The Effect of summer tropical heating on the location and intensity of the extratropical westerly jet streams," *Journal of Geophysical Research*, vol. 95, no. 11, pp. 18705–18721, 1990.

[28] B. Xiang and B. Wang, "Mechanisms for the advanced Asian summer monsoon onset since the mid-to-late 1990s," *Journal of Climate*, vol. 26, no. 6, pp. 1993–2009, 2013.

[29] X. Jiang, Y. Li, S. Yang, K. Yang, and J. Chen, "Interannual variation of summer atmospheric heat source over the Tibetan Plateau and the role of convection around the western Maritime Continent," *Journal of Climate*, vol. 29, no. 1, pp. 121–138, 2016.

[30] J. Shaman and E. Tziperman, "The effect of enso on Tibetan plateau snow depth: a stationary wave teleconnection mechanism and implications for the south asian monsoons," *Journal of Climate*, vol. 18, no. 12, pp. 2067–2079, 2005.

[31] W. Li, W. Guo, P. Hsu, and Y. Xue, "Influence of the Madden–Julian oscillation on Tibetan Plateau snow cover at the intraseasonal time-scale," *Scientific Reports*, vol. 6, no. 1, Article ID 30456, 2016.

[32] W. Li, W. Guo, B. Qiu, Y. Xue, P. Hsu, and J. Wei, "Influence of Tibetan Plateau snow cover on East Asian atmospheric circulation at medium-range time scales," *Nature Communications*, vol. 9, no. 1, p. 4243, 2018.

[33] X. Chen, D. Long, Y. Hong, S. Liang, and A. Hou, "Observed radiative cooling over the Tibetan Plateau for the past three decades driven by snow cover-induced surface albedo anomaly," *Journal of Geophysical Research, [Atmospheres]*, vol. 122, no. 12, pp. 6170–6185, 2017.

[34] L. Song, R. Wu, and L. An, "Different sources of 10- to 30-day intraseasonal variations of autumn snow over western and eastern Tibetan Plateau," *Geophysical Research Letters*, vol. 46, no. 15, pp. 9118–9125, 2019.

[35] W. Li, B. Qiu, W. Guo, Z. Zhu, and P. Hsu, "Intraseasonal variability of Tibetan Plateau snow cover," *International Journal of Climatology*, vol. 40, no. 7, pp. 3451–3466, 2020.

[36] G. Wu, H. Zhuo, Z. Wang, and Y. Liu, "Two types of summertime heating over the Asian large-scale orography and excitation of potentialvorticity forcing I. Over Tibetan Plateau," *Science China Earth Sciences*, vol. 59, no. 10, pp. 1996–2008, 2016.

[37] Z. Wang, A. Duan, G. Wu, and S. Yang, "Mechanism for occurrence of precipitation over the southern slope of the Tibetan Plateau without local surface heating," *International Journal of Climatology*, vol. 36, no. 12, pp. 4164–4171, 2016.

[38] Z. Wang, S. Yang, N. Lau, and A. Duan, "Teleconnection between summer NAO and East China rainfall variations: a bridge effect of the Tibetan Plateau," *Journal of Climate*, vol. 31, no. 16, pp. 6433–6444, 2018.

[39] Z. Wang, S. Yang, A. Duan, W. Hua, K. Ullah, and S. Liu, "Tibetan Plateau heating as a driver of monsoon rainfall variability in Pakistan," *Climate Dynamics*, vol. 52, no. 9-10, pp. 6121–6130, 2019.

[40] G. Wu, Y. Liu, B. He, Q. Bao, A. Duan, and F. Jin, "Thermal controls on the Asian summer monsoon," *Scientific Reports*, vol. 2, no. 1, p. 404, 2012.

[41] Z. Xie and A. Duan, "Relationship between the Tibetan plateau heat source and convection over the philippine sea (in Chinese)," *Chinese Journal of Atmospheric Sciences*, vol. 41, pp. 811–830, 2017.

[42] Z. Wang, S. Yang, H. Luo, and J. Li, "Drying tendency over the southern slope of the Tibetan Plateau in recent decades: role of a CGT-like atmospheric change," *Climate Dynamics*, vol. 59, no. 9-10, pp. 2801–2813, 2022.

[43] L. Dai and T. Che, "Cross-platform calibration of SMMR, SSM/I and AMSR-E passive microwave brightness temperature," in *Sixth International Symposium on Digital Earth: Data Procession and Applications*, H. D. Guo and C. L. Wang, Eds., vol. 7841, Bellingham, WA, USA, International Society for Optical Engineering SPIE Proceedings, Article ID 784103, 2010.

[44] L. Dai, T. Che, and Y. Ding, "Inter-calibrating SMMR, SSM/I and SSMI/S data to improve the consistency of snow-depth products in China," *Remote Sensing*, vol. 7, no. 6, pp. 7212–7230, 2015.

[45] M. Yanai, S. Esbensen, and J.-H. Chu, "Determination of bulk properties of tropical cloud clusters from large-scale heat and moisture budgets," *Journal of the Atmospheric Sciences*, vol. 30, no. 4, pp. 611–627, 1973.

[46] M. Ting and L. Yu, "Steady response to tropical heating in wavy linear and nonlinear baroclinic models," *Journal of the Atmospheric Sciences*, vol. 55, no. 24, pp. 3565–3582, 1998.

[47] C. Fu and Q. Wang, "The definition and detection of the abrupt climatic change (in Chinese)," *Chinese Journal of Atmospheric Sciences*, vol. 16, pp. 482–493, 1992.

[48] J. Ge, Q. You, and Y. Zhang, "The influence of the Asian summer monsoon onset on the northward movement of the South Asian high towards the Tibetan Plateau and its

thermodynamic mechanism," *International Journal of Climatology*, vol. 38, no. 2, pp. 543–553, 2018.

[49] P. Webster and S. Yang, "Monsoon and Enso: selectively interactive systems," *Quarterly Journal of the Royal Meteorological Society*, vol. 118, no. 507, pp. 877–926, 1992.

[50] S. Yang, K. Deng, and W. Duan, "Selective interaction between monsoon and ENSO: effects of annual cycle and spring predictability barrier (in Chinese)," *Chinese Journal of Atmospheric Sciences*, vol. 42, pp. 570–589, 2018.

[51] B. Liu, C. Zhu, and Y. Yuan, "Two interannual dominant modes of the South Asian high in May and their linkage to the tropical SST anomalies," *Climate Dynamics*, vol. 49, no. 7-8, pp. 2705–2720, 2017.

[52] M. Potocki, P. Mayewski, T. Matthews et al., *Npj Climate and Atmospheric Science*, vol. 5, no. 1, p. 7, 2022.

[53] C. Zhang, Z. Zheng, Y. Ou et al., "The evolution of snow depth over the southern Tibetan plateau in late spring to early summer and roles of the air temperature(pre-print)," *Research Square*, 2022.